I&EC research
Industrial & Engineering Chemistry Research
pubs.acs.org/IECR
Article

Understanding the Reaction Kinetics and Microdynamics between Methylimidazole and Alkyl Thiocyanate for Ionic Liquid Synthesis through Experiments and Theoretical Calculation

Fan Zhang, Weizhong Zheng,* Fan Yang, Zhihong Ma, Weizhen Sun,* and Ling Zhao

Cite This: *Ind. Eng. Chem. Res.* 2023, 62, 3889−3897
Read Online
ACCESS | Metrics & More | Article Recommendations

ABSTRACT: Ionic liquids (ILs) are usually prepared via the Menshutkin S_N2 reaction. Herein, the effects of the alkyl chain length of the substrate on the reaction kinetics and microdynamics between 1-methylimidazole (MIm) and alkyl thiocyanate (RSCN, R = methyl, ethyl, and butyl groups) for the preparation of thiocyanate-based ILs were analyzed by time-dependent Fourier transform infrared (FTIR) spectroscopy, classical molecular dynamics (MD) simulation, and ab initio molecular dynamics (AIMD) simulation. Experimental results show that the longer chain length of thiocyanate leads to a significantly slower rate constant and much higher activation energy. The rate constant of the MIm/BuSCN system is reduced by a factor of 21 fold compared to that of the MIm/MeSCN system at 330 K. The activation energy of the MIm/BuSCN system is increased by 27.5 kJ/mol in the MIm/MeSCN system. Metadynamics calculations in the explicit solvent offer a consistent trend for transition state energy barrier with experiments. MD simulations indicate that the long alkyl chain of thiocyanate results in a weaker spatial distribution of reaction sites as well as slower diffusion and reorientation, which can reduce the intermolecular collision probability. Hopefully, the insights from this work would guide the industrial synthesis of ILs.

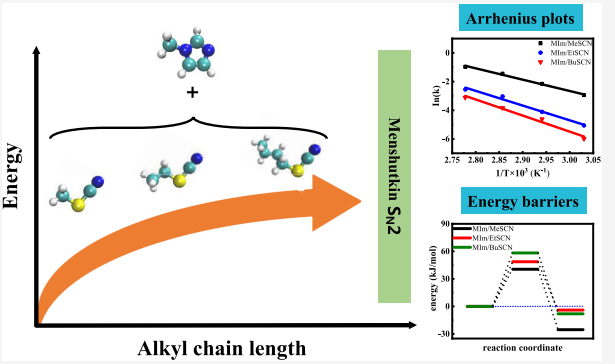

1. INTRODUCTION

Ionic liquids (ILs), composed exclusively of ions, have considerable applications in the fields such as catalysis,[1,2] extraction, and separation due to their negligible vapor pressure, high ionic conductivity, large temperature stability, and good solvent properties.[3−5] For a given application, the properties of ILs can be easily tuned by different cations and anions.[6,7] In particular, the alkyl chain length of cations plays an important role in the properties of ILs, including density, conductivity, surface tension, and diffusion coefficient.[8,9] However, the synthesis of ILs with a long alkyl chain usually takes a very long reaction time.[10] For example, the reaction of aniline derivatives with a long alkyl chain requires a long time of 2−7 days at 70 °C without reaction kinetics parameters.[11]

ILs are commonly synthesized by two neutral reactants to form oppositely charged ions, which belong to the Menshutkin S_N2 reaction.[12−18] There are several reports on the reaction kinetics of the synthesis of ILs. For example, Schleicher et al. studied the preparation of 1-hexyl-3-methylimidazoline bromide in 10 different solvents with emphasis on the solvent effects on the reaction kinetics.[19] Böwing et al. investigated the reaction kinetics between ethylmethylimidazole and ethylsulfate for the synthesis of ILs using different reactor types.[20] In contrast, Appetecchi et al. reported the synthesis of $PYR_{1A}TFSI$ (A = C_nH_{2n+1}, n from 1 to 10) to investigate the effect of alkyl chain length on the conductivity of ILs.[9] However, the reaction kinetics of these ILs was not studied. Lerch et al. synthesized ILs containing bromino or bis(trifluoromethane)sulfonimide anions and 1-aryl-3-alkylimidazole cations with different substituents at the *ortho* and *para* positions of the benzene ring and alkyl chains varying from butyl to dodecyl group.[11] However, their study only reported the effect of alkyl chain length on their physical properties, and no detailed kinetic data were available. Given the increasing applications of ILs, the effect of the substrate with different alkyl chain lengths on the reaction kinetics of the synthesis of ILs needs more attention, especially from the industrial point of view. Furthermore, few studies have addressed the underlying microscopic structure, dynamics, and reaction behaviors that affect the reaction kinetics[21] of the reactants with different alkyl chain lengths for the preparation of ILs.

Received: December 1, 2022
Revised: February 15, 2023
Accepted: February 15, 2023
Published: February 24, 2023

https://doi.org/10.1021/acs.iecr.2c04323
Ind. Eng. Chem. Res. 2023, 62, 3889−3897

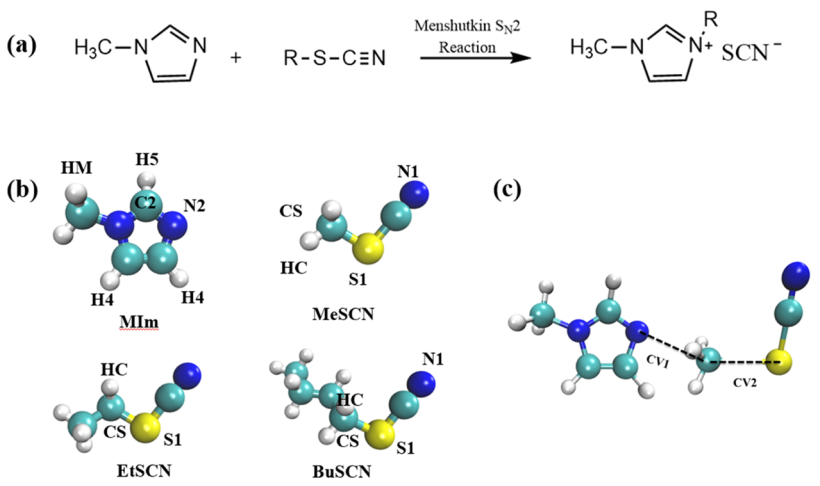

Figure 1. (a) Reaction between MIm and RSCN (R = C_nH_{2n+1}, n = 1, 2, 4) for the preparation of thiocyanate-based IL. (b) Optimized molecular structures of MIm, MeSCN, EtSCN, and BuSCN with atom labels. (c) Selection of collective variables for metadynamics calculations.

Alternatively, MD simulation and AIMD simulation are currently used as promising tools for studying the complex structure, dynamics, and reaction behaviors at a molecular level. Neumann et al. used MD simulations to study a variety of properties of ILs composed of 1-alkyl-3-methylimidazole cations and bis(trifluoromethylsulfonylimine) anions ([C_nMIm][NTf_2], n = 2, 4, 6, 8), such as density, diffusion coefficient, vaporization enthalpy, reorientation correlation time, and viscosity.[22] Sun et al. conducted MD simulations on the cycloaddition reaction catalyzed by PIL ([HDBU][MIm]) and APIL ([MeDBU][MIm]) and explored the catalytic mechanism of PIL ([HDBU][MIm] and APIL ([MeDBU]-[MIm]) for the cycloaddition reaction of CO_2 and PO. Based on the activation energy barrier of the rate-determining step, the optimal reaction route was obtained.[2] Reddy et al.[23] investigated the structural and kinetic properties of conjugated cationic liquid mixtures using MD simulations. The structural evolution of the mixtures was represented by radial distribution function (RDF), coordination number, void analysis, and spatial distribution function (SDF). Brehm et al.[24] investigated the structure of the 1-ethyl-3-methylimidazole acetate and water mixtures at different water contents by calculating the structure, hydrogen bonding, and characteristic bond length and angles of cations and anions. Fu et al. probed the effect of acceptors and solvents on the mechanism of glycosylation reactions using AIMD simulations in explicit solvent, and the reaction free energy was simulated based on metadynamics calculations.[25]

The reaction process between MIm and alkyl thiocyanate (RSCN) for the preparation of thiocyanate-based ILs, as shown in Figure 1a, was chosen as the object of the present study since the C≡N bonds in the reactants and products have strong infrared characteristic peaks and can be easily characterized.[26] More importantly, ILs synthesized from imidazole and thiocyanate have important applications in the extraction of model oils for deep desulfurization,[27] separation of cresols from coal tar,[28] and as corrosion inhibitors for the steel in H_2SO_4 and HCl media.[29] Thus, in this work, the effects of the alkyl chain length of substrate thiocyanate on reaction kinetics and microdynamics between MIm and thiocyanate with methyl, ethyl, and butyl groups (MeSCN, EtSCN, BuSCN) for the synthesis of thiocyanate-based ILs were investigated by means of in situ FTIR, AIMD and MD simulations. Specifically, the reaction rates and reaction activation energies were obtained by in situ FTIR characterization. The experimental results indicate that the increased alkyl chain length leads to a significant decrease in the reaction rate and an obvious increase in the activation energy. The energy barrier calculated by metadynamics calculation follows a trend similar to the experiment. In addition, MD simulations reveal that both diffusion and reorientation dynamics of molecules in the reaction system slow down with increasing alkyl chain length of the substrate, which also leads to a decrease in the reaction rate.

2. EXPERIMENTAL PROCEDURES AND MD DETAILS

2.1. Sample Preparation. MIm and alkyl thiocyanate (MeSCN, EtSCN, BuSCN) were mixed in a scintillation vial at a 20:1 molar ratio in a glovebox and stirred for 5 min. The obtained mixed sample was then assembled in an FTIR sample cell. FTIR spectra were acquired every 15 min for the initial 4 h at a given temperature. Then, the sample was heated up to 360 K, and the spectra were taken every day until the reaction was completed. The resultant time-dependent spectra of the CN stretching mode were used to compute the fractional yields of SCN^- during the process.[26]

2.2. MD Details. The optimized structures of MIm, MeSCN, EtSCN, and BuSCN are shown in Figure 1b. All of the initial boxes were built with Packmol.[30] For MD simulations, the number of MIm and thiocyanate (MeSCN, EtSCN, BuSCN) molecules was 400 and 20, respectively. The box size of MIm/MeSCN, MIm/EtSCN, and MIm/BuSCN systems was 35.0 × 34.3 × 34.0 $Å^3$, 34.0 × 34.8 × 35.0 $Å^3$, and 33.9 × 34.5 × 35.9 $Å^3$, respectively. For the obtained MIm/MeSCN, MIm/EtSCN, and MIm/BuSCN boxes, 10,000 steps of energy minimization were first taken. Then, a 5 ns run under constant-volume (*NVT*) ensemble with a Nose−Hoover thermostat[31,32] was conducted, followed by a 40 ns run under isobaric-isothermal (*NPT*) ensemble with a Parrinello−Rahman barostat[33,34] at 360 K for equilibration. For MD systems, the last 15 ns trajectories were employed to analyze the structure and dynamics properties of interest. The cubic periodic boxes of dimension 13.7 × 13.7 × 13.7 $Å^3$ containing 20 MIm molecules and 1 thiocyanate molecule were also modeled and equilibrated using the same steps to provide the pre-equilibrated structures for subsequent AIMD simulations.

https://doi.org/10.1021/acs.iecr.2c04323
Ind. Eng. Chem. Res. 2023, 62, 3889−3897

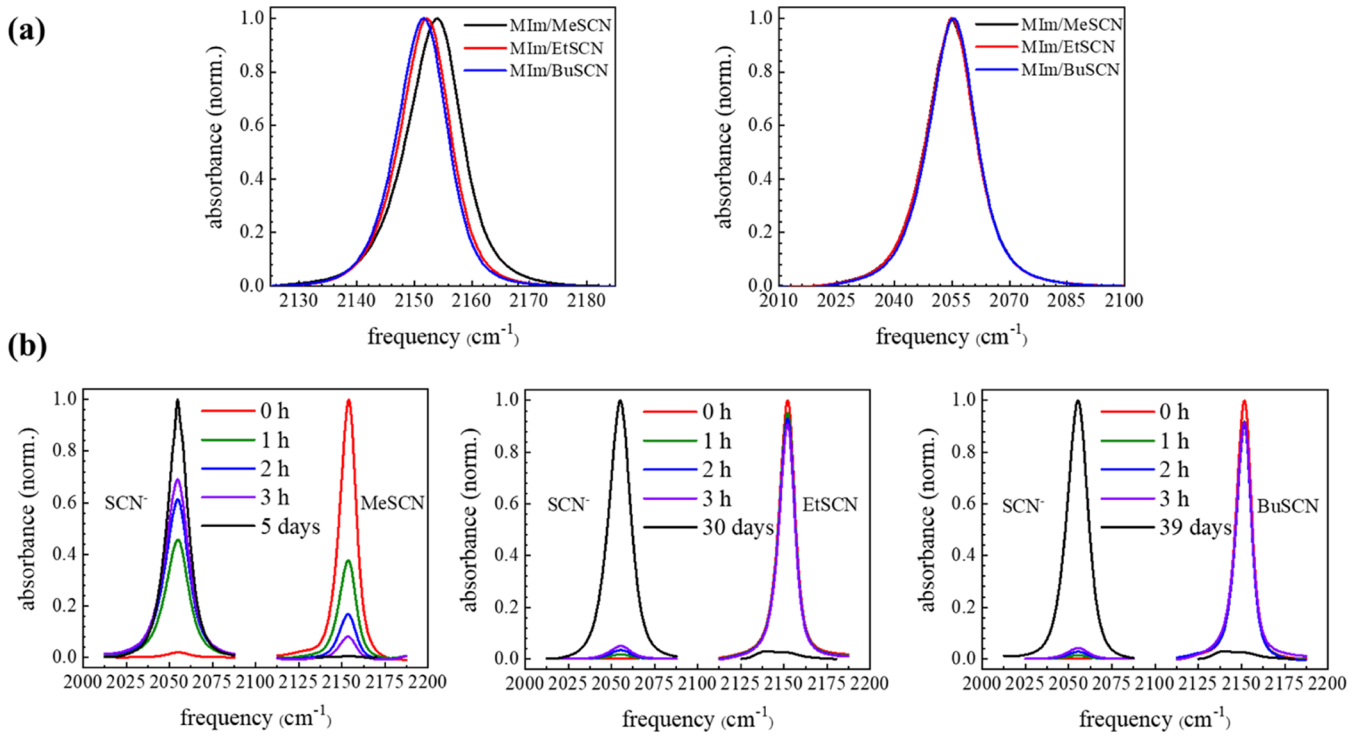

Figure 2. (a) Normalized, background-subtracted FTIR spectra of the CN stretching modes of RSCN and SCN^-. (b) Time-dependent normalized and background-subtracted FTIR spectra of RSCN and SCN^- at 340 K.

The Lennard–Jones (L–J) potential was used to describe the interactions between the MIm and MeSCN, EtSCN, and BuSCN molecules. The parameters taken from the OPLS-AA force field were employed to represent the MIm and thiocyanate molecules, in which the L–J parameters for the C and N atoms on the CN groups of thiocyanate molecules were described by the ANL model.[35] More importantly, the SCN group of the thiocyanate molecules was modified by the virtual atom (VA) with the total mass of C and N atoms to be set on the VA atom according to the same moment of inertia. The optimized structures of MIm, MeSCN, EtSCN, and BuSCN were obtained at the B3LYP/6–311G(d,p) level, and the ChelpG charges were refitted at the same level using the Gaussian 09 program.[36] All of the MD simulations were conducted with the GROMACS program.[37,38] The time step for all of the simulations was set to be 1 fs. The periodic boundary conditions were used in three dimensions with Lorentz–Berthelot mixing rules. The long-range electrostatic interactions were treated by the particle mesh Ewald method with a cutoff radius of 1.2 nm. The initial velocities were randomly generated from a Maxwell–Boltzmann distribution, and the LINCS algorithm was utilized to constrain the covalent bonds including hydrogen atoms.

2.3. Metadynamics Calculations. The equilibrated configurations containing 20 MIm and 1 RSCN from the above MD simulations were further prepared using AIMD simulations for 10 ps before Metadynamics-based free energy surface calculations. All of the AIMD simulations and Metadynamics calculations were performed using CP2K simulations. The Gaussian and plane wave (GPW) method with Goedecker–Teter–Hutter pseudopotentials[39] was used. The DZVP-MOLOPT-GTH basis set was used for all atoms with a cutoff energy of 400 Ry.[40] The GGA-PBE method was used to process the exchange–correlation function supplemented with the Grimme D3 dispersion correction, and the convergence thresholds for the total energy and SCF calculations were kept at 10^{-10} and 10^{-8} hartree, respectively.[41] For the structural optimization and transition state calculations, the gradient and displacement convergence criteria were set to 5×10^{-5} hartree/bohr and 1×10^{-4} bohr, respectively. Metadynamics calculations were performed for 50 ps to obtain the two-dimensional (2D) free energy surface of the reaction process of MIm and thiocyanate molecules at 360 K.[42,43] The CS–N2 distance and CS–S1 distance are used as collective variables. The first collective variable (CV1) follows the bond formation between the carbon (CS) on the alkyl thiocyanate chain and the nitrogen atom (N2) on the nucleophile (MIm). The second collective variable (CV2) follows the broken bond between CS and the sulfur atom on the leaving group of thiocyanate (SCN) (Figure 1c). For both collective variables, repulsive Gaussian situation mounds with a height of 0.3 kcal/mol and a width of 0.1 were added to the potential every 50 molecular dynamics steps. At the same time, the harmonic restraint with force constant k = 0.005 and TARGET = 0.2 nm was used to keep the distance of CVs from going too far.

3. RESULTS AND DISCUSSION

3.1. FTIR Spectrum. The normalized background-subtracted CN stretch vibrations of the RSCN and SCN^- with different alkyl chain lengths are compared, as shown in Figure 2a. The band centers of MeSCN and SCN^- are consistent with previous studies.[26] From Figure 2a, the alkyl chain length of thiocyanate has little effect on the SCN^- peak center at 2054.8 cm^{-1}. The peak centers of MeSCN, EtSCN, and BuSCN are 2154.0, 2152.2, and 2151.6 cm^{-1}, respectively. A red shift of the peak center of RSCN was observed with increasing alkyl chain length. This is attributed to the decrease

https://doi.org/10.1021/acs.iecr.2c04323
Ind. Eng. Chem. Res. 2023, 62, 3889–3897

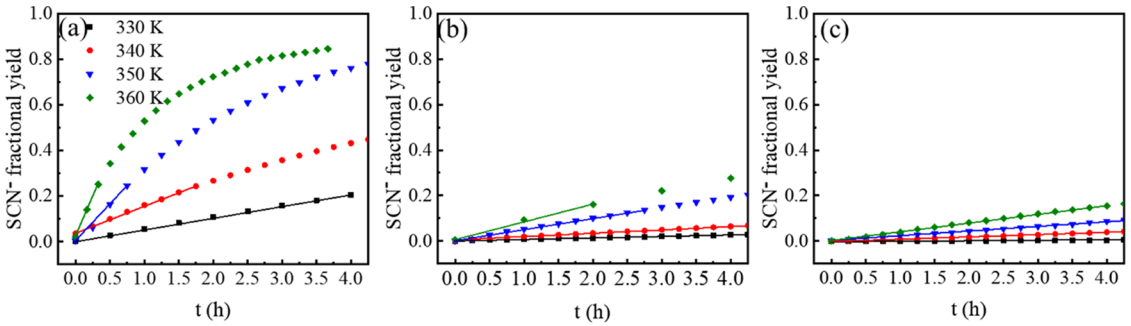

Figure 3. Time-dependent fractional yield of SCN^- in (a) MIm/MeSCN, (b) MIm/EtSCN, and (c) MIm/BuSCN as a function of temperature. The dot is the experimental value, and the solid line represents the linear fitting.

Table 1. Temperature-Dependent Rate Constant and Activation Energies in Each System

	rate constants $k \times 10^{-2}$ (h^{-1})							E_a (kJ/mol)	A (h^{-1})
	300 K	310 K	320 K	330 K	340 K	350 K	360 K	330–360 K	
MIm/MeSCN	0.452	1.076	2.840	5.274	11.585	23.555	38.119	65.8	1.42×10^9
MIm/EtSCN			0.284	0.633	1.638	4.822	7.816	85.4	2.23×10^{11}
MIm/BuSCN				0.250	1.093	2.166	4.449	93.3	1.72×10^{12}

of the electrophilicity of the active carbon atoms (CS) of the longer alkyl chains, which causes the shift of the IR absorption peaks toward the lower frequencies.

Monitoring the time-dependent spectrum of the RSCN and SCN^- nitrile stretch bands provides time-dependent concentrations of these species.[26] Figure 2b shows the time-dependent normalized spectra of MeSCN and SCN^- at 340 K. Note that the peak of the initial MeSCN spectrum is used to normalize the MeSCN spectra, and the SCN^- spectra are normalized based on the final one. With the progress of the reaction, the peak area of MeSCN decreases, and the peak area of SCN^- increases. After a considerable amount of time, the MeSCN peak totally vanishes, and the SCN^- peak reaches the maximum value, indicating that the reaction is finished. From Figure 2b, it takes about 30 and 39 days to react completely for the EtSCN and BuSCN, respectively. These results provide a valuable reference for IL preparation with a longer alkyl chain.

3.2. Rate Constant. Figure 3 shows the fractional yield of SCN^- with different alkyl chain lengths as a function of temperature over time. The fractional yield of SCN^- is less than 20% in 3 h in the MIm/MeSCN system at 330 K, while it is slightly below 5% in the MIm/EtSCN system and MIm/BuSCN system. The reaction proceeds more rapidly at elevated temperatures. For example, the MIm/MeSCN system yields of up to 80% are obtained at 360 K. The increase of SCN^- can be approximated as linear in a short time. To obtain the reaction rate, a linear fitting of the early data was used, as shown in Figure 3.

Table 1 lists the rate constants k obtained from the slope of the fitting line based on pseudo first order. The k of the MIm/MeSCN system increases 26 fold at 340 K relative to 300 K, well consistent with the 25-fold increase in k of the imidazole-based IL reaction with increasing temperature from 298.2 to 333.2 K.[19] The reaction of the MIm/EtSCN system at 300 and 310 K is very slow and difficult to observe. Similarly, the reaction of the MIm/BuSCN system at 300–320 K was also extremely slow. Furthermore, the rate constant declines rapidly with increasing alkyl chain length of thiocyanate molecules in the temperature range studied. Specifically, the rate constant of the MIm/EtSCN system is reduced by a factor of 8 fold compared to that of the MIm/MeSCN system at 330 K. At the same temperature, the rate constant of the MIm/BuSCN system is reduced by a factor of 21 fold and by a factor of 3 fold compared to that of MIm/MeSCN and MIm/EtSCN systems, respectively. These indicate that the reaction rate for the preparation of thiocyanate-based ILs was significantly reduced by the increased alkyl chain length of the substrate. It is more noteworthy that the reaction rate decreases sharply when the alkyl chain is switched from methyl to ethyl group, but only a slight decrease in the reaction rate when switching from ethyl to butyl group. This may be due to the additional length, as well as the additional conformers that are spatially distant from the transition state and leaving group.[44]

The rate constant of the thermal activation process with temperature can be described by the Arrhenius equation

$$k = A e^{-E_a/RT} \quad (1)$$

in which A, E_a, and R are the pre-exponential factor, the activation energy, and the ideal gas constant, respectively. The effect of the alkyl chain length of the substrate on the reaction activation energy is further quantified in Figure 4, which shows a plot of ln k vs $1/T$. A linear fit was performed on the data

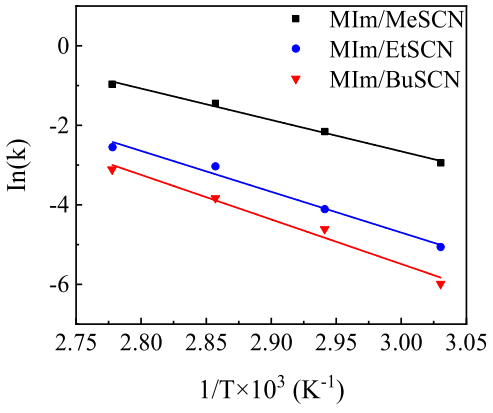

Figure 4. Arrhenius plots for the MIm/MeSCN, MIm/EtSCN, and MIm/BuSCN systems.

https://doi.org/10.1021/acs.iecr.2c04323
Ind. Eng. Chem. Res. 2023, 62, 3889–3897

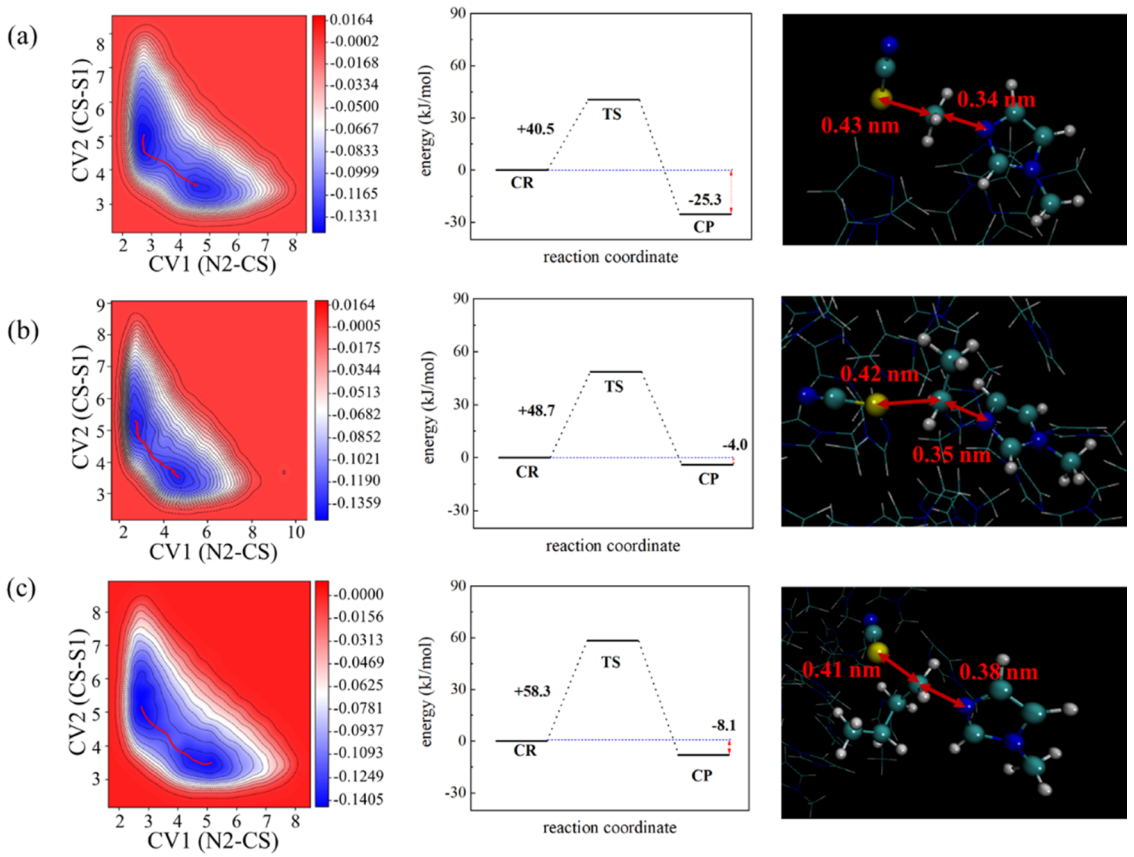

Figure 5. 2D free energy surface, energy barriers, and the geometries of transition states. (a) MIm/MeSCN, (b) MIm/EtSCN, and (c) MIm/BuSCN. The zero energy reference point of the system is the energy of the corresponding CR.

from 330 to 360 K to derive A and E_a from the intercept and slope. The activation energies of the MIm/MeSCN, MIm/EtSCN, and MIm/BuSCN systems are 65.8, 85.4, and 93.3 kJ/mol, respectively. The activation energy increases with the increased alkyl chain length of the substrate.

3.3. Reaction Energy Profile. To further examine the effect of the alkyl chain length of thiocyanate on the reaction, the free energy calculations based on the metadynamics calculation in explicit liquid-phase environments for the reaction systems with different chain lengths of substrate were conducted. The free energy surfaces in metadynamics calculation are reconstructed from a small number of selected collective variables (CVs).[45] The bias potential of the distance is introduced after the cleavage of N2−CS and the formation of CS−S1 bonds, which are used as collective variables.

Figure 5 shows the two-dimensional (2D) free energy surface (FES), energy barriers, and geometries of transition states (TS) for MIm/MeSCN, MIm/EtSCN, and MIm/BuSCN. From the results of the FES, it is well consistent with a concerted S_N2 reaction path for all three reaction systems. The minimum energy path (MEP) on the FES and the TS configurations suggest that the cleavage of the CS−S1 bond and the formation of the CS−N2 bond occur synchronously without the formation of a carbenium intermediate. The energy barrier ΔE^* is the energy difference between TS and CR along the MEP, in which the reactant binding complex (CR) is the zero energy reference point for reaction calculations. The energy of the product binding complex (CP) in relation to CR is the reaction energy (ΔE^R). For the MIm/MeSCN, MIm/EtSCN, and MIm/BuSCN systems, the ΔE^* values calculated in the explicit liquid-phase environments were 40.5, 48.7, and 58.3 kJ/mol, respectively. These values are smaller than the ΔE^* of 121.5 kJ/mol calculated for the gas phase between MIm and MeSCN,[26] since the solvent effect is considered using metadynamics calculations. ΔE^* increases with the increasing alkyl chain length of thiocyanate, which is qualitatively consistent with the experimental results. The calculated energy barrier for the MIm/EtSCN system increases by about 20% relative to the MIm/MeSCN system. The TS structures reveal that the reaction between MIm and RSCN tends to follow the back-side substitution (S_N2-b) pathway because, in most circumstances, the front-side substitution (S_N2-f) pathway is particularly unfavorable due to the steric repulsion between the nucleophilic fraction and the leaving group. Similarly, the MIm/BuSCN system increases the potential barrier by about 20% relative to the MIm/EtSCN system. The main reason for the difference in ΔE^* is that as the electron-donating effect of larger alkyl chains increases and the electrophilicity of the active carbon atoms decreases, making them less susceptible to nucleophilic attack.[46] In addition, as the length of the alkyl chain increases, the distance of the CS−S1 bond decreases, and the distance of the CS−N2 bond increases. The decrease in the distance between CS and S1 at the bond break and the increase in the distance between CS and N2 at the bond formation in the transition state structure are also consistent with this description.

3.4. Microstructure. To further analyze the microstructure features of the reaction system, the spatial distribution function (SDF) and radial distribution function (RDF) were calculated

https://doi.org/10.1021/acs.iecr.2c04323
Ind. Eng. Chem. Res. 2023, 62, 3889−3897

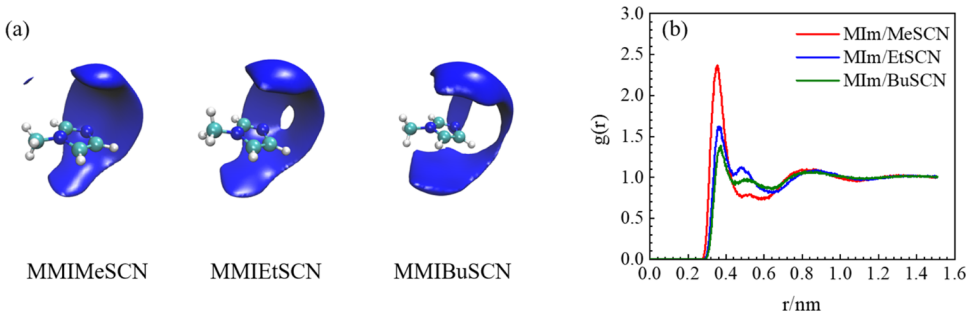

Figure 6. SDF of thiocyanate around MIm in different systems and RDF between N2 atoms of MIm molecules and CS atoms of thiocyanate molecules.

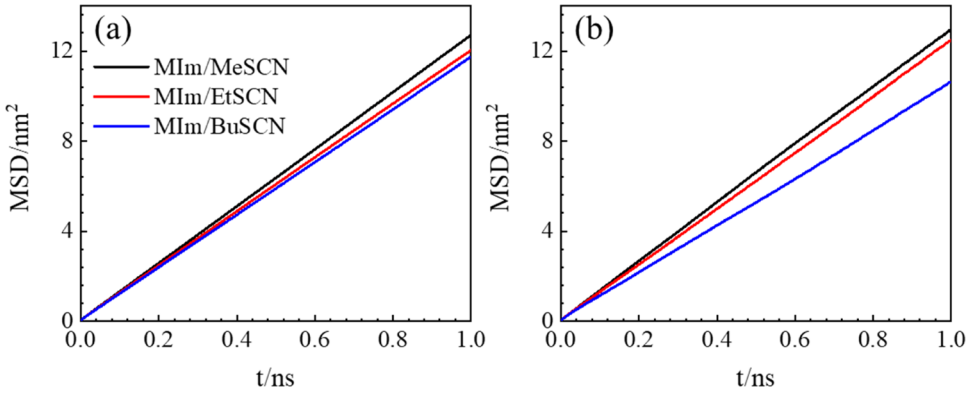

Figure 7. MSD curves of (a) MIm and (b) RSCN with time in different systems.

using the TRAVIS[47] package. The SDF of thiocyanate around MIm in different systems is presented in Figure 6a. As for the MIm/MeSCN system, MeSCN molecules tend to point slightly more toward the vertical position of the imidazole ring of MIm and around the N2 atom. With the increase in the alkyl chain length of thiocyanate, the distribution of EtSCN molecules and BuSCN molecules around the N2 atom of the MIm molecule decreases and BuSCN molecule tends to be distributed parallel to the imidazole ring of MIm, which suggests that the EtSCN and BuSCN have a smaller probability to react with N2 atoms.

To further analyze the influence of the alkyl chain length of thiocyanate on the microstructure characteristics, the RDFs between N2 atoms on MIm molecules and CS atoms on thiocyanate molecules were also calculated, as shown in Figure 6b. As for the MIm/MeSCN system, the peak of RDF N2−CS is relatively sharp with a value greater than 2. However, the height of the first peak of RDF in MIm/EtSCN and MIm/BuSCN systems decreases, and the first maximum value of RDF is less than 2. As the alkyl chain of thiocyanate is prolonged, the location of RDFs becomes larger. Specifically, the first maximum peak is located at a distance of 0.354 nm in the MIm/MeSCN system, but it is located at 0.368 nm in the MIm/EtSCN system and 0.372 nm in the MIm/BuSCN system. The corresponding peak intensities in these three systems are 2.37, 1.62, and 1.38, respectively. Generally speaking, the distribution probability of CS around N2 is relatively higher in the MIm/MeSCN system because the long alkyl chain of thiocyanate shows a larger steric effect and results in a decrease in the distribution of thiocyanate around the MIm molecule, well consistent with the results of SDFs. Thus, it can be concluded that the steric effect of the substrate leads to a change in the relative distribution between MIm and thiocyanate molecules, thus affecting the reactivity between the reactant molecules.

3.5. Microdynamics. In addition to the microstructure characteristics, microdynamics was also studied. Aiming to get further insight into the microdynamics behaviors of the systems, the mean squared displacement (MSD) of MIm, MeSCN, EtSCN, and BuSCN as a function of time is calculated using the following equation

$$\mathrm{MSD} = \langle |x(t) - x(0)|^2 \rangle = \frac{1}{N}\sum_{i=1}^{N} |x_i(t) - x_i(0)|^2 = t^{\beta} \tag{2}$$

where β describes the mode of motion. According to the Einstein equation, in a three-dimensional system, the correlation of the self-diffusion coefficient (D) and MSD can be described as

$$D = \frac{1}{6}\lim_{\Delta t \to \infty} \frac{\mathrm{dMSD}}{\mathrm{d}\Delta t} \tag{3}$$

The D can be obtained by the slope of the MSD−t curve. The MSDs of MIm, MeSCN, EtSCN, and BuSCN in all of the systems at 360 K are linearly dependent on time, as shown in Figure 7a,b. It is observed that the MSDs decrease with increasing alkyl chain length of thiocyanate, which corresponds to a slower diffusion. The quantitative D of the molecules in each system was calculated in the time range of 0−4.0 ns, as shown in Figure 8. At 360 K, D_{MIm} is 1.256×10^{-9} m^2/s and D_{MeSCN} is 1.308×10^{-9} m^2/s in the MIm/MeSCN system, but D_{MIm} is 1.186×10^{-9} m^2/s and D_{BuSCN} is 1.060×10^{-9} m^2/s in the MIm/BuSCN system. The D of MIm is less than that of MeSCN in the MIm/MeSCN system, but in the MIm/BuSCN system, the D of MIm is greater than that of BuSCN. As the

https://doi.org/10.1021/acs.iecr.2c04323
Ind. Eng. Chem. Res. 2023, 62, 3889−3897

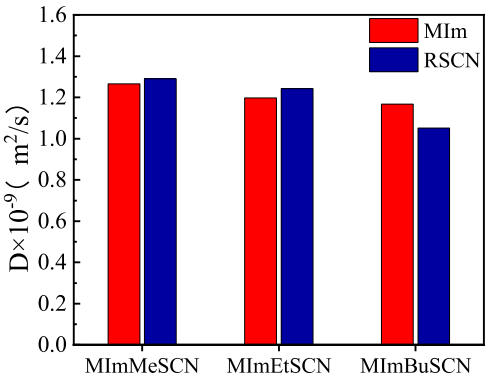

Figure 8. Self-diffusion coefficients of MIm and thiocyanate molecules from MD simulations at 360 K.

alkyl chain length of the substrate increases from methyl to butyl group, the D of MIm decreased by 6%, while the D of BuSCN decreased by 19% compared with that of MeSCN. Clearly, the longer alkyl chains of thiocyanate molecules result in the slower dynamics of the systems.

Reorientation $(C(t))$ is used to investigate the rotational dynamics of ions. Figure 9 shows the rotational dynamics of the C−N vector of RSCN and the N−N vector of MIm at 360 K. The reorientation of methylimidazole is less influenced by the alkyl thiocyanate due to a 20-fold excess of imidazole. However, with the increased alkyl chain length of thiocyanate, the $C(t)$ decay of the C−N vector of thiocyanate becomes slower, indicating that the reorientation of RSCN molecules slows down. For example, the decay of $C(t)$ of the C−N vector of thiocyanate is completed within 20 ps in the MIm/MeSCN system, but in the MIm/BuSCN system, it needs about 40 ps. Thus, the larger substrate chain length leads to slower reorientation dynamics.

The reorientation anisotropy of MIm and thiocyanate in MIm/MeSCN, MIm/EtSCN, and MIm/BuSCN systems is well described by double exponential fitting, and the corresponding parameters are listed in Table 2. The increase in the alkyl chain length of thiocyanates leads to a slower second time scale (t_2). t_2 shows an increased trend with the increased thiocyanate chain length, which suggests that t_2 is sensitive to the substrate chain length. The integrated correlation time (τ_c) is also included in Table 2, which is calculated by

$$\tau_c = \frac{1}{A(0)} \int_0^\infty A(t)\mathrm{d}t \tag{4}$$

where $A(t)/A(0)$ represents the normalized correlation function. The τ_c of MIm tends to increase with the alkyl chain length of thiocyanate. The τ_c of BuSCN at 360 K is about 1.8 times higher than that of MeSCN. The obviously increased τ_c is seen with the increase of the thiocyanate alkyl chain. Generally, the increased alkyl chain length of the substrate causes the slower diffusion and reorientation of the reactants for the synthesis of ILs, leading to a reduction in the collision probability and thus the reaction rate.

4. CONCLUSIONS

In this work, the reaction kinetics of the Menshutkin S_N2 reaction between MIm and thiocyanates of different chain lengths was investigated by in situ FTIR spectroscopy and AIMD and MD simulations. Pseudo-first-rate constants were obtained from the CN stretching absorption growth of SCN^- in a system, and the longer alkyl chain length of thiocyanates results in a smaller rate constant. At 330−360 K, the activation energy of the MIm/BuSCN system is 7.9 kJ/mol higher than that of the MIm/EtSCN system, and the activation energy of the MIm/EtSCN system is 19.6 kJ/mol higher than that of the MIm/MeSCN system. The energy barrier obtained from metadynamics calculations increases with increasing chain length, which follows the same trend as the activation energy obtained from experiments.

In terms of MD simulations, the distribution of RSCN molecules around the N2 atom of the MIm molecule decreases as the length of the thiocyanate alkyl chain increases, tending to be distributed parallel to the MIm molecular plane. The large substrate groups of thiocyanate molecules lead to significantly slower reorientation and diffusion dynamics. The D of all molecules declines gradually with the increase of the alkyl chain of the thiocyanate substrate. Based on the results of $C(t)$, the attenuation time of BuSCN molecules in the MIm/BuSCN system is almost twice slower than that of MeSCN molecules in the MIm/MeSCN system. A longer alkyl chain length of the substrate leads to slower molecular motion, reducing the probability of intermolecular collisions. The basic viewpoint of this work contributes to a better understanding of the mechanism by which the alkyl chain length of thiocyanate regulates the synthesis of thiocyanate-based ILs, guiding the industrial synthesis of ILs with different chain lengths.

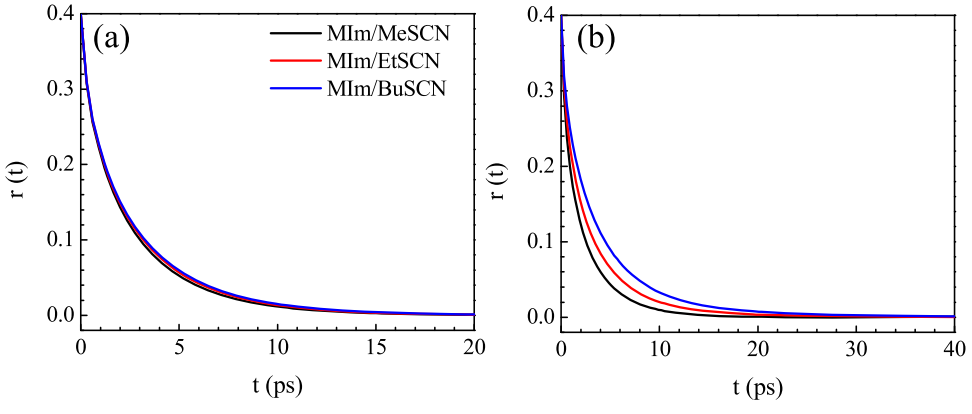

Figure 9. Reorientation dynamics of the N−N vector of MIm (a) and the C−N vector of RSCN (b) in different systems.

https://doi.org/10.1021/acs.iecr.2c04323
Ind. Eng. Chem. Res. 2023, 62, 3889−3897

Table 2. Orientational Relaxation Parameters in MIm/MeSCN, MIm/EtSCN, and MIm/BuSCN Systems at 360 K

system	sample	A_1	t_1(ps)	A_2	t_2(ps)	τ_c(ps)
MIm/MeSCN	MIm-NN	0.128	0.459	0.271	3.08	0.905
	MeSCN-CN	0.166	0.482	0.233	3.02	0.798
MIm/EtSCN	MIm-NN	0.128	0.470	0.270	3.25	0.951
	EtSCN-CN	0.161	0.619	0.234	4.03	1.10
MIm/BuSCN	MIm-NN	0.130	0.483	0.268	3.38	0.986
	BuSCN-CN	0.142	0.733	0.251	4.99	1.43

AUTHOR INFORMATION

Corresponding Authors

Weizhong Zheng − *State Key Laboratory of Chemical Engineering, School of Chemical Engineering, East China University of Science and Technology, Shanghai 200237, China;* orcid.org/0000-0002-3866-4932; Email: sunwz@ecust.edu.cn

Weizhen Sun − *State Key Laboratory of Chemical Engineering, School of Chemical Engineering, East China University of Science and Technology, Shanghai 200237, China;* orcid.org/0000-0002-9957-3620; Email: wzzheng@ecust.edu.cn

Authors

Fan Zhang − *State Key Laboratory of Chemical Engineering, School of Chemical Engineering, East China University of Science and Technology, Shanghai 200237, China*

Fan Yang − *State Key Laboratory of Chemical Engineering, School of Chemical Engineering, East China University of Science and Technology, Shanghai 200237, China*

Zhihong Ma − *State Key Laboratory of Chemical Engineering, School of Chemical Engineering, East China University of Science and Technology, Shanghai 200237, China*

Ling Zhao − *State Key Laboratory of Chemical Engineering, School of Chemical Engineering, East China University of Science and Technology, Shanghai 200237, China;* orcid.org/0000-0001-5239-1152

Complete contact information is available at: https://pubs.acs.org/10.1021/acs.iecr.2c04323

Notes

The authors declare no competing financial interest.

ACKNOWLEDGMENTS

The financial support from the National Natural Science Foundation of China (22008065 and 91434108) is gratefully acknowledged.

REFERENCES

(1) Li, M.; Chen, J.; Li, L.; Ye, C.; Lin, X.; Qiu, T. Novel multi−SO_3H functionalized ionic liquids as highly efficient catalyst for synthesis of biodiesel. *Green Energy Environ.* **2021**, *6*, 271−282.

(2) Sun, W.; Wang, M.; Zhang, Y.; Ding, W.; Huo, F.; Wei, L.; He, H. Protic vs aprotic ionic liquid for CO_2 fixation: A simulation study. *Green Energy Environ.* **2020**, *5*, 183−194.

(3) Ghandi, K. A review of ionic liquids, their limits and applications. *Green Sustainable Chem.* **2014**, *04*, 44−53.

(4) Marsh, K. N.; Boxall, J. A.; Lichtenthaler, R. Room temperature ionic liquids and their mixtures—a review. *Fluid Phase Equilib.* **2004**, *219*, 93−98.

(5) Freemantle, M. *An Introduction to Ionic Liquids*; Royal Society of Chemistry, 2010.

(6) Wu, J.; Zhang, L.; Long, J.; Zeng, Q.; Yin, B.; Li, X. Synthesis and fluorescent properties of quinoxaline derived ionic liquids. *Green Energy Environ.* **2022**, *7*, 996−1005.

(7) Yuan, X.; Liu, J.; Qin, J.; Ma, W.; Liu, G.; Wang, Y.; He, H. Smart ionic liquid/water mixture system with dual stimuli-response to temperature and CO_2. *Nano Res.* **2022**, 1−8.

(8) Yeganegi, S.; Sokhanvaran, V.; Soltanabadi, A. Study of thermodynamic properties of imidazolium-based ionic liquids and investigation of the alkyl chain length effect by molecular dynamics simulation. *Mol. Simul.* **2013**, *39*, 1070−1078.

(9) Appetecchi, G. B.; Montanino, M.; Zane, D.; Carewska, M.; Alessandrini, F.; Passerini, S. Effect of the alkyl group on the synthesis and the electrochemical properties of N-alkyl-N-methyl-pyrrolidinium bis(trifluoromethanesulfonyl)imide ionic liquids. *Electrochim. Acta* **2009**, *54*, 1325−1332.

(10) Wasserscheid, P.; Welton, T. *Ionic Liquids in Synthesis*; Wiley Online Library, 2008.

(11) Lerch, S.; Strassner, T. Synthesis and Physical Properties of Tunable Aryl Alkyl Ionic Liquids (TAAILs). *Chem. - Eur. J.* **2021**, *27*, 15554−15557.

(12) Halls, M. D.; Schlegel, H. B. Chemistry inside carbon nanotubes: the Menshutkin S_N2 reaction. *J. Phys. Chem. B* **2002**, *106*, 1921−1925.

(13) Alkorta, I.; Elguero, J. The S_N2 reaction and its relationship with the Walden inversion, the Finkelstein and Menshutkin reactions together with theoretical calculations for the Finkelstein reaction. *Struct. Chem.* **2021**, *32*, 1755−1761.

(14) Chandrasekhar, J.; Smith, S. F.; Jorgensen, W. L. Theoretical examination of the S_N2 reaction involving chloride ion and methyl chloride in the gas phase and aqueous solution. *J. Am. Chem. Soc.* **1985**, *107*, 154−163.

(15) Vayner, G.; Houk, K. N.; Jorgensen, W. L.; Brauman, J. I. Steric retardation of S_N2 reactions in the gas phase and solution. *J. Am. Chem. Soc.* **2004**, *126*, 9054−9058.

(16) Bento, A. P.; Solà, M.; Bickelhaupt, F. M. Ab initio and DFT benchmark study for nucleophilic substitution at carbon (S_N2@ C) and silicon (S_N2@ Si). *J. Comput. Chem.* **2005**, *26*, 1497−1504.

(17) Mikosch, J.; Trippel, S.; Eichhorn, C.; Otto, R.; Lourderaj, U.; Zhang, J.; Hase, W.; Weidemuller, M.; Wester, R. Imaging nucleophilic substitution dynamics. *Science* **2008**, *319*, 183−186.

(18) Shaik, S. S.; Schlegel, H. B.; Wolfe, S. *Theoretical Aspects of Physical Organic Chemistry: The S_N2 Mechanism*; Wiley, 1992.

(19) Schleicher, J. C.; Scurto, A. M. Kinetics and solvent effects in the synthesis of ionic liquids: imidazolium. *Green Chem.* **2009**, *11*, 694−703.

(20) Böwing, A. G.; Jess, A. Kinetics and reactor design aspects of the synthesis of ionic liquids—Experimental and theoretical studies for ethylmethylimidazole ethylsulfate. *Chem. Eng. Sci.* **2007**, *62*, 1760−1769.

(21) Espenson, J. H. *Chemical Kinetics and Reaction Mechanisms*; McGraw-Hill, 1995.

(22) Neumann, J.; Golub, B.; Odebrecht, L.-M.; Ludwig, R.; Paschek, D. Revisiting imidazolium based ionic liquids: Effect of the conformation bias of the [NTf_2] anion studied by molecular dynamics simulations. *J. Chem. Phys.* **2018**, *148*, No. 193828.

(23) Reddy, T. D. N.; Mallik, B. S. Hydrogen Bond Kinetics, Ionic Dynamics, and Voids in the Binary Mixtures of Protic Ionic Liquids with Alkanolamines. *J. Phys. Chem. B* **2021**, *125*, 5587−5600.

(24) Brehm, M.; Weber, H.; Pensado, A. S.; Stark, A.; Kirchner, B. Proton transfer and polarity changes in ionic liquid-water mixtures: a perspective on hydrogen bonds from ab initio molecular dynamics at the example of 1-ethyl-3-methylimidazolium acetate-water mixtures–part 1. *Phys. Chem. Chem. Phys.* **2012**, *14*, 5030−5044.
(25) Fu, Y.; Bernasconi, L.; Liu, P. Ab Initio Molecular Dynamics Simulations of the S_N1/S_N2 Mechanistic Continuum in Glycosylation Reactions. *J. Am. Chem. Soc.* **2021**, *143*, 1577−1589.
(26) Zheng, W.; Yamada, S. A.; Hung, S. T.; Sun, W.; Zhao, L.; Fayer, M. D. Enhanced menshutkin S_N2 reactivity in mesoporous silica: the influence of surface catalysis and confinement. *J. Am. Chem. Soc.* **2020**, *142*, 5636−5648.
(27) Gao, L.; Wan, H.; Han, M.; Guan, G. Deep desulfurization of model oil by extraction with a low-viscosity ionic liquid [BMIM]SCN. *Pet. Sci. Technol.* **2014**, *32*, 1309−1317.
(28) Li, A.; Xu, X.; Zhang, L.; Gao, J.; Xu, D.; Wang, Y. Separation of cresol from coal tar by imidazolium-based ionic liquid [EMIM]-[SCN]: Interaction exploration and extraction experiment. *Fuel* **2020**, *264*, No. 116908.
(29) Corrales-Luna, M.; Le Manh, T.; Romero-Romo, M.; Palomar-Pardavé, M.; Arce-Estrada, E. M. 1-Ethyl 3-methylimidazolium thiocyanate ionic liquid as corrosion inhibitor of API 5L X52 steel in H_2SO_4 and HCl media. *Corros. Sci.* **2019**, *153*, 85−99.
(30) Martínez, L.; Andrade, R.; Birgin, E. G.; Martínez, J. M. PACKMOL: a package for building initial configurations for molecular dynamics simulations. *J. Comput. Chem.* **2009**, *30*, 2157−2164.
(31) Nosé, S. A unified formulation of the constant temperature molecular dynamics methods. *J. Chem. Phys.* **1984**, *81*, 511−519.
(32) Hoover, W. G. Canonical dynamics: Equilibrium phase-space distributions. *Phys. Rev. A* **1985**, *31*, 1695−1697.
(33) Parrinello, M.; Rahman, A. Polymorphic transitions in single crystals: A new molecular dynamics method. *J. Appl. Phys.* **1981**, *52*, 7182−7190.
(34) Nosé, S.; Klein, M. L. Constant pressure molecular dynamics for molecular systems. *Mol. Phys.* **1983**, *50*, 1055−1076.
(35) Gee, P. J.; van Gunsteren, W. F. Acetonitrile revisited: a molecular dynamics study of the liquid phase. *Mol. Phys.* **2006**, *104*, 477−483.
(36) Frisch, M.; Trucks, G.; Schlegel, H.; Scuseria, G.; Robb, M.; Cheeseman, J.; Scalmani, G.; Barone, V.; Mennucci, B.; Petersson, G. *Gaussian 09*, Revision D. 01; Gaussian, Inc.: Wallingford CT, 2009.
(37) Van Der Spoel, D.; Lindahl, E.; Hess, B.; Groenhof, G.; Mark, A. E.; Berendsen, H. J. GROMACS: fast, flexible, and free. *J. Comput. Chem.* **2005**, *26*, 1701−1718.
(38) Hess, B.; Kutzner, C.; Van Der Spoel, D.; Lindahl, E. GROMACS 4: algorithms for highly efficient, load-balanced, and scalable molecular simulation. *J. Chem. Theory Comput.* **2008**, *4*, 435−447.
(39) Allolio, C.; Klameth, F.; Vogel, M.; Sebastiani, D. Ab initio H_2O in realistic hydrophilic confinement. *ChemPhysChem* **2014**, *15*, 3955−3962.
(40) Comas-Vives, A. Amorphous SiO_2 surface models: energetics of the dehydroxylation process, strain, ab initio atomistic thermodynamics and IR spectroscopic signatures. *Phys. Chem. Chem. Phys.* **2016**, *18*, 7475−7482.
(41) Caratelli, C.; Hajek, J.; Rogge, S. M.; Vandenbrande, S.; Meijer, E. J.; Waroquier, M.; Van Speybroeck, V. Influence of a Confined Methanol Solvent on the Reactivity of Active Sites in UiO-66. *ChemPhysChem* **2018**, *19*, 420−429.
(42) Laio, A.; Parrinello, M. Escaping free-energy minima. *Proc. Natl. Acad. Sci. U.S.A.* **2002**, *99*, 12562−12566.
(43) Hutter, J.; Iannuzzi, M.; Schiffmann, F.; VandeVondele, J. Cp2k: atomistic simulations of condensed matter systems. *Wiley Interdiscip. Rev.: Comput. Mol. Sci.* **2014**, *4*, 15−25.
(44) Schleicher, J. *Kinetics and Solvent Effects in the Synthesis of Ionic Liquids*; University of Kansas, 2007.
(45) Barducci, A.; Bonomi, M.; Parrinello, M. Metadynamics. *Wiley Interdiscip. Rev.: Comput. Mol. Sci.* **2011**, *1*, 826−843.
(46) Jug, U.; Pregeljc, D.; Mavri, J.; Vianello, R.; Stare, J. Elementary S_N2 reaction revisited. Effects of solvent and alkyl chain length on kinetics of halogen exchange in haloalkanes elucidated by Empirical Valence Bond simulation. *Comput. Theor. Chem.* **2017**, *1116*, 96−101.
(47) Brehm, M.; Kirchner, B. TRAVIS-a free analyzer and visualizer for Monte Carlo and molecular dynamics trajectories. *J. Chem. Inf. Model.* **2011**, *51*, 2007−2023.

https://doi.org/10.1021/acs.iecr.2c04323
Ind. Eng. Chem. Res. 2023, 62, 3889−3897